

A comparative study of different active heave compensation approaches

Shrenik Zinage^{*} and Abhilash Somayajula^a

Department of Ocean Engineering, Indian Institute of Technology Madras, Chennai, India

(Received September 6, 2020, Revised November 24, 2020, Accepted December 10, 2020)

Abstract. Heave compensation is a vital part of various marine and offshore operations. It is used in various applications, including the transfer of cargo between two vessels in the open ocean, installation of topsides of an offshore structure, offshore drilling and for surveillance, reconnaissance and monitoring. These applications typically involve a load suspended from a hydraulically powered winch that is connected to a vessel that is undergoing dynamic motion in the ocean environment. The goal in these applications is to design a winch controller to keep the load at a regulated height by rejecting the net heave motion of the winch arising from ship motions at sea. In this study, we analyze and compare the performance of various control algorithms in stabilizing a suspended load while the vessel is subjected to changing sea conditions. The KCS container ship is chosen as the vessel undergoing dynamic motion in the ocean. The negative of the net heave motion at the winch is provided as a reference signal to track. Various control strategies like Proportional-Derivative (PD) Control, Model Predictive Control (MPC), Linear Quadratic Integral Control (LQI), and Sliding Mode Control (SMC) are implemented and tuned for effective heave compensation. The performance of the controllers is compared with respect to heave compensation, disturbance rejection and noise attenuation.

Keywords: active heave compensation; winch control; PD; MPC; LQI; SMC

1. Introduction

With an increasing demand for various resources, mankind has started to look to the oceans, that are rich in several minerals and other natural resources. In order for these resources to be extracted, various processes like deep sea mining and offshore drilling are used (Ni *et al.* 2009, Korde 1998, Woodacre 2015, Woodacre *et al.* 2015). Deep sea mining is the process of retrieving the mineral deposits from the ocean floor. The National Institute of Ocean Technology (NIOT) in India (Atmanand and Ramadass 2017) is currently planning to extract such minerals from the Central Indian Ocean Basin (CIOB) located at a depth of 6000 meters. NIOT is currently building a crawler based mining machine that can collect, crush, and pump the mineral nodules to the mother ship (Atmanand and Ramadass 2017). This operation is generally executed by suspending a mine excavator from a surface vehicle. For effective mining, the heave motion of the vessel needs to be compensated.

^{*}Corresponding author, B.Tech., E-mail: shrenikvz@gmail.com

^a Ph.D., E-mail: abhilash@iitm.ac.in

External disturbances like waves, winds, and currents can cause the vessel to experience strong dynamic motion in both seakeeping (vertical plane motion) and maneuvering modes (horizontal plane motions). The maneuvering motions are slower (of the order of a few minutes) and the seakeeping modes are faster (of the order of a few seconds). The maneuvering modes of motion can generally be controlled effectively using dynamic positioning systems (Fossen 2011, Fossen and Strand 2001, Sørensen 2005, Grimble *et al.* 1980). However, the seakeeping motions of the vessel need effective compensation to achieve regulation of the payload position.

Heave compensation approaches can be classified into two main categories: passive heave compensation (PHC) and active heave compensation (AHC). A PHC device functions as a vibration absorber that is tuned to absorb the energy at certain range of frequencies. It is used on existing or new lifting devices to reduce the dynamic load. These systems generally do not require a power supply for their operation. However, the compensation performance through PHC systems is typically around 80 % (Hatleskog and Dunnigan 2007).

On the other hand, AHC system is an active feedback system that provides the payload displacement as a feedback to the controller at every time instant so that a better compensation is achieved (Woodacre *et al.* 2015, Li *et al.* 2012). This type of feedback based compensation requires a significant power source for its functioning. AHC systems are vulnerable to external and internal perturbances like variation of payload, nonlinear friction and unmodelled winch dynamics (Jakubowski and Milecki 2018). Over the years various control algorithms have been suggested for achieving AHC (Zhao *et al.* 2018, Li *et al.* 2019).

AHC systems are composed of controllers that use the feedback signal to provide an actuation signal through actuators. Actuators are mechanical devices driven by electric motors and usually suffer from saturation. This means that there is a limit on the maximum actuation that can be achieved from an actuator. A lot of research is currently underway on handling a payload when actuators are subjected to saturation and disturbances (Galuppini *et al.* 2018).

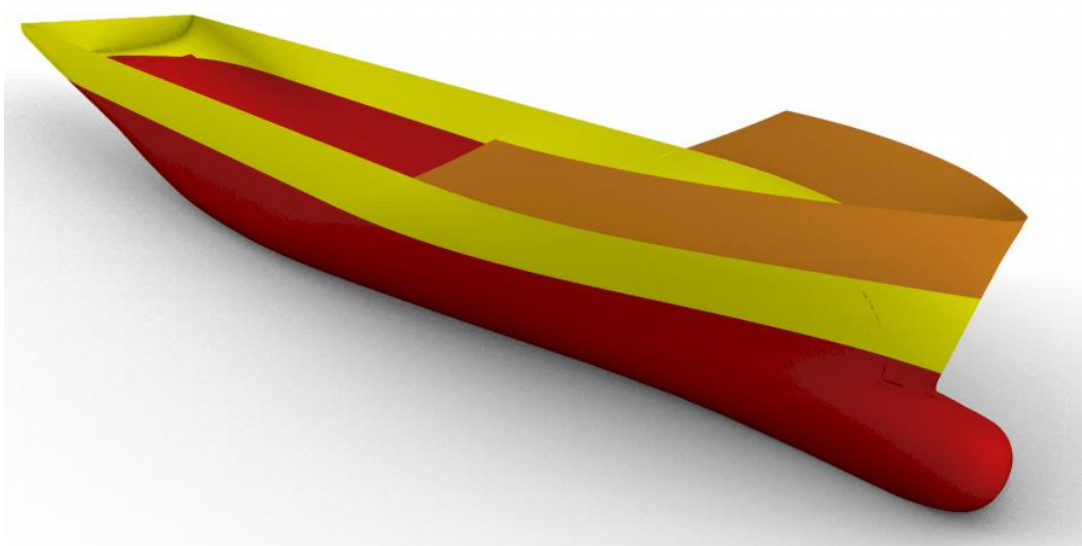


Fig. 1 KCS Container Ship

Table 1 KCS Particulars

Particulars	Value
Length between perpendiculars L_{pp}	230 m
Length waterline L_{WL}	232.5 m
Breadth B	32 m
Depth D	19 m
Draft T	10.8 m
Displacement	52030 m ³
Block Coefficient C_B	0.65
LCB from midship (fwd +)	-3.404 m
LCB from AP (fwd +)	111.596 m
VCG from WL	3.551 m
VCG from keel	14.351 m
GM	0.6 m
Design Forward Speed U	24 knots
Analysis Speed (In this study)	0 knots
Froude Number F_n	0.259927
Roll Radius of gyration about CG k_{xx}	12.88 m
Pitch/Yaw radius of gyration about CG k_{yy}/k_{zz}	57.5 m

In this study the KCS vessel is chosen and the net heave motion at an on-board winch due to combined heave, roll, and pitch motion is calculated for three sea states. Fig. 1 shows the hull form of KCS container ship. Table 1 shows the particulars of an KCS ship. The negative of the net heave time history is given as a reference signal to the controller that drives an actuator. The actuator then controls the unwound rope of the compensation winch. The compensated motion of the payload is then given as the summation of the vessel's net heave response and the unwound rope length and denotes the motion of the payload after compensation.

In this study, various control strategies for AHC are investigated and compared. It is assumed that the system is of strict feedback form without an observer and the cable does not lose tension throughout the operation. The rest of the paper is organized into five sections. Section 2 describes the modeling of ship motion in waves. The dynamic model of the winch is described in Section 3. The different AHC control strategies compared in this study are described in Section 4. Section 5 describes the results and the conclusions are provided in Section 6.

2. Ship motion modeling

The Pierson Moskowitz spectrum corresponding to a significant wave height H_s and peak period T_p for a range of frequencies is defined by

$$S(\omega) = \frac{0.3125}{2\pi} T_p H_s^2 \left(\frac{\omega T_p}{2\pi}\right)^{-5} \exp\left(\frac{-5}{4} \left(\frac{\omega T_p}{2\pi}\right)^{-4}\right) \quad (1)$$

For a simulation duration of T seconds, the frequency increment is given by $\Delta\omega = 2\pi/T$. At each discrete frequency $\omega_n = n\Delta\omega$, the amplitude of the n^{th} wave component is given by

$$A_n = \sqrt{2S(\omega_n)\Delta\omega} \quad (2)$$

The initial phase ϕ_n of each wave component is sampled from a uniform distribution between $-\pi$ and π . This method of computing wave elevation time history from spectrum is known as random phase method (Somayajula 2017). After calculating A_n , ω_n is revised by randomization within a $\Delta\omega$ interval to avoid the signal from repeating itself. The random values of frequencies are chosen as shown in Eq. (3)

$$(\omega_n)_{\text{new}} = (\omega_n)_{\text{old}} + \Delta\omega X \quad (3)$$

where X is a random variable following a uniform distribution between -0.5 and 0.5. The resultant irregular wave elevation time history is given by

$$\eta(t) = \sum_{i=1}^N A_n \cos(\omega_n t + \phi_n) \quad (4)$$

where N is the number of wave components. In this study N is taken as 100001 to simulate a 10000 s time history with a sampling time of 0.1 s.

The random wave elevation time history as per Eq. (4) was calculated for the following three sea states:

1. Rough sea state: $H_s = 5.9$ m, $T_p = 12$ s
2. Moderate sea state: $H_s = 4$ m, $T_p = 9$ s
3. Slight sea state: $H_s = 1.5$ m, $T_p = 6$ s

The plot of the PM spectrum for these three sea states is shown in Fig. 2. The response amplitude operator (RAO) of the KCS container ship is obtained for the heave, roll and pitch modes using MDLHydroD developed by Guha (2016) (Somayajula *et al.* 2014, Guha *et al.* 2016) which is a frequency domain 3D panel method based tool for analysis of wave structure interaction. Although the frequency domain program is capable of including forward speed effects, forward speed was not considered in this study for AHC. The magnitude of heave, roll and pitch RAOs of the KCS container ship for a wave incident angle of 135 degrees are shown in Fig. 3.

It can be seen that the RAO of roll exhibits a sharp peak, which corresponds to a low potential damping at the roll natural frequency of the vessel. In such cases, viscous damping plays a significant role. This is usually estimated from physical model tests (Somayajula and Falzarano 2016, 2017a, b) or from empirical relationships (Falzarano *et al.* 2015).

It can be seen that the RAO of roll exhibits a sharp peak, which corresponds to a low potential damping at the roll natural frequency of the vessel. In such cases, viscous damping plays a significant role. This is usually estimated from physical model tests (Somayajula and Falzarano 2016, 2017a, b) or from empirical relationships (Falzarano *et al.* 2015). However, in this study, the viscous roll damping has not been considered on purpose to enhance the motion of the vessel and thus observe and compare the effectiveness of various controllers in keeping the load suspended from an on-board winch stabilized.

After the RAO is obtained, the response spectrum of the roll, pitch and heave is calculated as shown below

$$S_{\text{response}}(\omega) = |H(\omega)|^2 S(\omega) \quad (5)$$

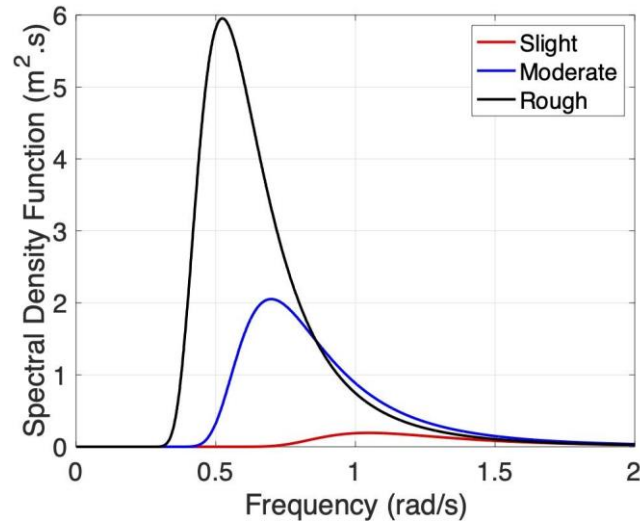


Fig. 2 PM Spectrum for 3 sea states

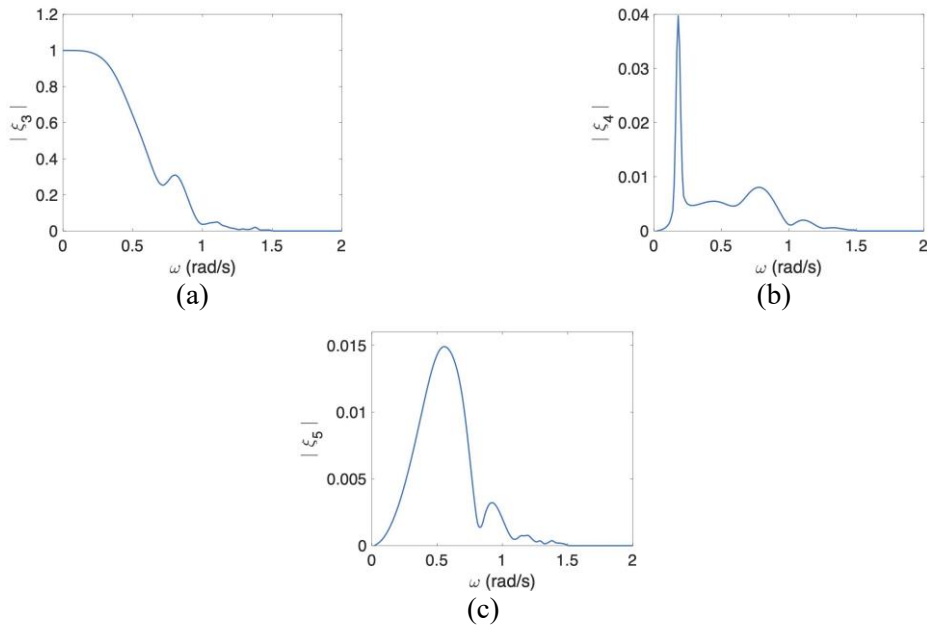


Fig. 3 (a) Heave RAO (b) Roll RAO (c) Pitch RAO

where $S_{response}$ is the response spectrum, $H(\omega)$ is the response RAO and $S(\omega)$ is the wave spectrum. Now the input wave elevation time history was decomposed into its frequency components by taking a fast Fourier transform (FFT). The amplitude of the response at a frequency $\omega_k = (k - 1)\Delta\omega$ is then obtained by taking the product of response RAO at that frequency and the FFT of input wave

elevation time history at the same frequency. Although a time history may contain several frequencies, we can only distinguish frequencies between 0 and the Nyquist frequency. The Nyquist frequency is half the sampling rate of the discrete signal and is given by $\omega_{nyq} = \pi/\Delta t$ where $\Delta t = 0.1$ sec. When a signal is sampled such that the frequency content in the signal is beyond the Nyquist frequency, the period of the sampled signal is observed to be larger than the period of the original signal. Therefore, when computing the time history of heave, roll and pitch motions, we only consider the frequencies less than the Nyquist frequency. The values at higher frequencies are taken to be mirrored conjugates of the values before the Nyquist frequency and the mirroring happens about the Nyquist frequency. Finally, inverse fast Fourier transform (IFFT) is used to convert these degrees of freedom back into time domain.

In this study, the origin of the ship fixed coordinate system was assumed to be at the intersection of the waterline, centerline, and midship. Assuming that the crane is placed at (x_{crane}, y_{crane}) in the vessel's body fixed coordinate system with a slewing gear angle β_s and the wave incident angle of β , the net heave response time history of the winch placed on board the KCS container ship is calculated in terms of the combined roll, heave, and pitch motion caused due to sea excitation. Fig. 4 shows a schematic diagram of the ship with a crane installed on it.

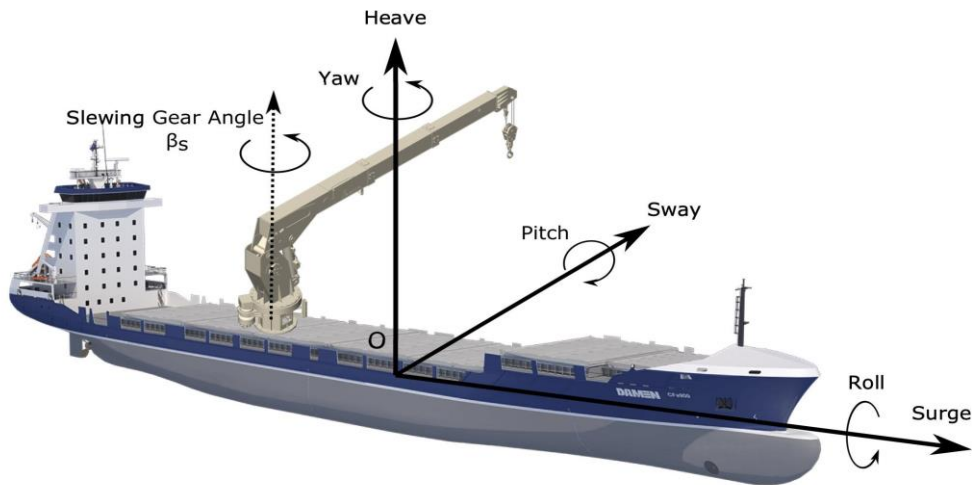


Fig. 4 Ship with Installed Crane (O is the intersection point of the waterline, centerline and midship)

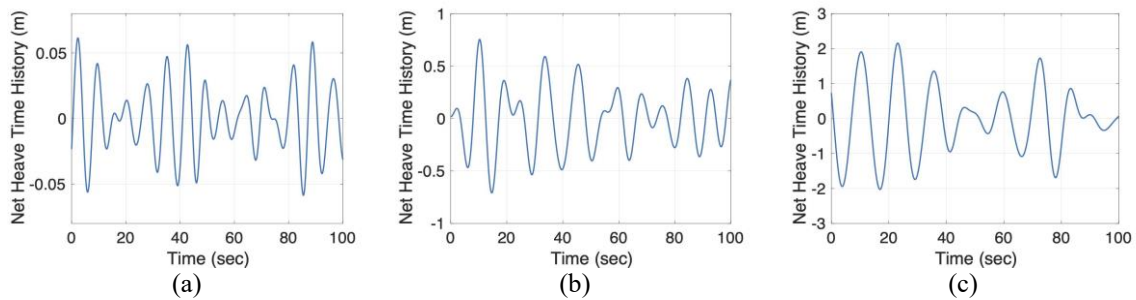


Fig. 5 (a) $H_s = 1.5$ m, $T_p = 6$ sec (b) $H_s = 4$ m, $T_p = 9$ sec (c) $H_s = 5.9$ m, $T_p = 12$ sec

Assuming small amplitude motions consistent with linear hydrodynamic theory, the net heave motion time history is given by

$$z_{winch} = \eta_3(\beta) + (y_{crane} + l_{crane}\sin(\beta_s))\eta_4(\beta) - (x_{crane} + l_{crane}\cos(\beta_s))\eta_5(\beta) \quad (6)$$

where $\eta_3(\beta)$, $\eta_4(\beta)$, and $\eta_5(\beta)$ are the heave, roll and pitch time histories respectively, which depend on the incident wave angle β . In this study, the coordinate of the crane with respect to vessel's body frame was assumed to be at (-1.5 m, 2 m) with a slewing gear angle of 73 degrees and the horizontal extent of the crane (l_{crane}) is assumed to be 3 m. The plot of a 100 second snip of the net heave motion time history in 3 different sea states when the waves are incident at an angle of 135 degrees are shown in Fig. 5.

3. Model of winch

In this paper the state space model for hydraulic drive of the winch is taken from Richter *et al.* (2017) for the implementation of various control strategies. A hydraulic winch is the most commonly used type of winch for active heave compensation of cranes because of its high power to weight ratio as compared to other motors like pneumatic motors, AC motors, DC motors etc.

A schematic diagram of the hydraulic drive is illustrated in Fig. 6. An electric motor drives the hydraulic pump with a constant angular speed ω_p that in turn drives the hydraulic motor with a variable angular speed ω_m depending on the normalized swash angle x_p of the pump. The motor here is assumed to be a fixed displacement motor with a displacement of D_m whereas the pump is assumed to be a variable displacement pump with a maximum displacement D_p . The displacement of the pump is controlled by a normalized swash angle ($-1 < x_p < 1$). Thus, the variation of normalized swash angle will govern the flow generated by the pump. A linear relationship is assumed between the normalized swash angle and the flow rate of the pump. The input to the plant is a control signal that translates to the normalized swash angle through a first order system. A saturation of normalized swash angle is assumed beyond $x_p = \pm 1$.

The connection between the pump and the motor is through hydraulic lines with volume V_c . The fixed displacement motor drives the winch to which the load is attached. Between the motor and the winch, a mechanical gear with a gear ratio k is placed. Proper oil supply is ensured with the help of

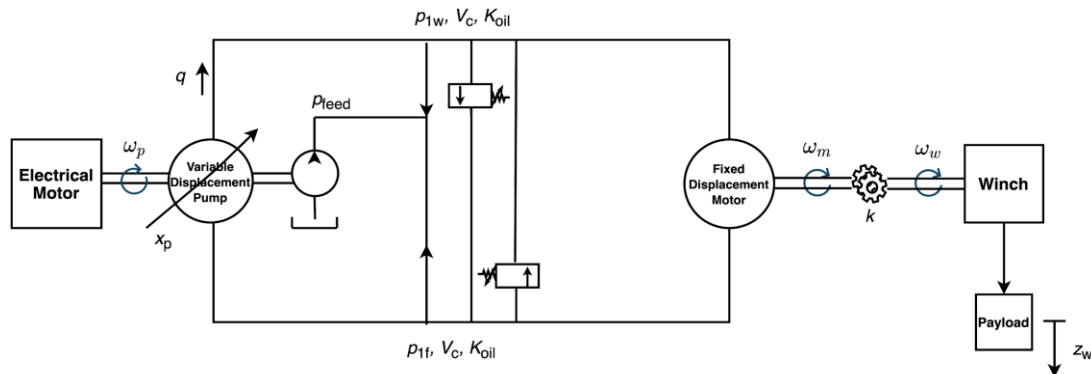


Fig. 6 Schematic diagram of hydraulic driven winch

feed pressure p_{feed} . The pressure relief valves make sure that the pressure doesn't cross safety limits. Since these limits are not usually reached in practice, the oil supply does not significantly affect the governing dynamics of the winch and hence the leakage of oil is not modeled in this study.

The compressibility of the hydraulic fluid is governed by the bulk modulus K_{oil} . The pressure on the either sides of the closed circuit is governed by

$$\begin{aligned}\dot{p}_{1w} &= \frac{K_{oil}}{V_c} (D_p \omega_p x_p - D_m \omega_m) \\ \dot{p}_{1f} &= \frac{K_{oil}}{V_c} (D_m \omega_m - D_p \omega_p x_p)\end{aligned}\quad (7)$$

where the pressure at the top and bottom hydraulic lines is denoted by p_{1w} and p_{1f} respectively.

Defining the change in pressure $\Delta p = p_{1f} - p_{1w}$, we have

$$\Delta \dot{p} = \frac{2K_{oil}}{V_c} (D_m \omega_m - D_p \omega_p x_p) \quad (8)$$

A negative constant swash angle x_p would yield a positive pressure Δp and negative flow rate q and vice versa. The equation for the dynamics of winch is governed by

$$(J_w + mr^2)\dot{\omega}_w = -D_m k \eta_m \Delta p - b \omega_w + mgr \quad (9)$$

where η_m denotes the efficiency of the motor, b denotes the viscous friction of the winch and ω_w denotes the rotational velocity of the winch with a radius r and inertia J_w . The relative position of the load with respect to the winch is denoted by z_w and the relative velocity is given by $\dot{z}_w = r \omega_w$. The torque due to the dynamics of lifting rope is neglected and the total torque is approximated by a constant payload torque mgr , where m is the mass of the payload and g is the acceleration due to gravity. The control input u_p and the normalized swash angle x_p are related through a first order system as shown in Eq. (10).

$$\dot{x}_p = \frac{-1}{T_w} (x_p - u_p) \quad (10)$$

where T_w is the time constant of the normalized swash plate. The state space model of the winch is given by

$$\begin{aligned}\dot{x} &= Ax + Bu_p + [0 \quad 0 \quad d \quad 0]^T \\ y &= z_w = Cx, \quad x(0) = x_0\end{aligned}\quad (11)$$

with the state

$$x = [x_p \quad \Delta p \quad \dot{z}_w \quad z_w]^T \quad (12)$$

the system matrix

$$A = \begin{bmatrix} -\frac{1}{T_w} & 0 & 0 & 0 \\ -\frac{2K_{oil}D_p\omega_p}{V_c} & 0 & \frac{2K_{oil}D_mk}{rV_c} & 0 \\ 0 & -\frac{rD_mk\eta_m}{J_w+mr^2} & -\frac{b}{J_w+mr^2} & 0 \\ 0 & 0 & 1 & 0 \end{bmatrix} \quad (13)$$

the input matrix

Table 2 Data values for the model of the winch

Parameter Name	Parameters	Value
Acceleration due to gravity	g	9.8 m/s^2
Bulk modulus of hydraulic fluid	K_{oil}	$1.8 \times 10^9 \text{ N/m}^2$
Volume of hydraulic lines	V_c	$2 \times 10^{-3} \text{ m}^3$
Maximum pump displacement	D_p	$40 \times 10^{-6} \text{ m}^3$
Fixed displacement of motor	D_m	$4 \times 10^{-6} \text{ m}^3$
Rotation rate of pump	ω_p	45 Hz
Time constant	T_w	1 s
Gear transmission ratio	k	200
Radius of winch	r	0.5 m
Efficiency of motor	η_m	0.65
Inertia of the winch	J_w	150 kgm^2
Viscous friction of the winch	b	$1 \times 10^4 \text{ kgm}^2/\text{s}$
Mass of the payload	m	1000 kg

$$B = \left[\frac{1}{T_w} \quad 0 \quad 0 \quad 0 \right]^T \quad (14)$$

the output matrix

$$C = [0 \quad 0 \quad 0 \quad 1] \quad (15)$$

and d is the disturbance which is caused due to unmodelled dynamics, nonlinear friction, vibrations and parameter uncertainty. The parameters for the hydraulic drive of the winch are shown in Table 2.

4. Controller design

4.1 PD Controller

PD Controller is one of the most common controllers used in several applications. Its advantages include fast rise time, proper reference tracking, and quick reaction to disturbances. In the marine industry, this controller is not only used in adjusting the heading angle of ships (Fang *et al.* 2012) and USVs (Sonnenburg and Woolsey 2013) but also has various uses in heave compensation (Li *et al.* 2018). In this paper, a PD controller was preferred over the PID controller because the plant already has an integrator which enables tracking without a steady state error.

The block diagram of the winch and the controller is shown in Fig. 7. The reference signal is taken as the opposite of the net heave motion time history so that the controller generates a control signal u_p in such a way that the output of the plant y tracks the opposite of the net heave time history r . This will ensure that the absolute motion of the payload is close to zero. The winch motion y is measured and fed back to the controller with the help of feedback sensor such as a winch encoder

which measures the actual length of rope that has been reeled in or out. The measured signal y_m is then given by the summation of the output and measurement noise.

Given a reference (r), disturbance (d), and measurement noise (n), the objective is to analyze the closed loop performance of the system. Based on Fig. 7, the Laplace transform of the governing differential equation of y and e can be written as

$$Y(s) = (1 + PC)^{-1}PCR(s) + (1 + PC)^{-1}D(s) - (1 + PC)^{-1}PCN(s) \quad (16)$$

$$E(s) = (1 + PC)^{-1}R(s) - (1 + PC)^{-1}D(s) + (1 + PC)^{-1}PCN(s) \quad (17)$$

where $Y(s)$, $R(s)$, $D(s)$, $N(s)$, and $E(s)$ are the Laplace transforms of $y(t)$, $r(t)$, $d(t)$, $n(t)$, and $e(t)$ respectively. $P(s)$ and $C(s)$ represents the plant and the controller transfer function in the Laplace domain. In practical applications, the disturbance is usually composed of low frequency components and the noise is composed of high frequency components. Let S be the sensitivity function representing the transfer function between disturbance and output, while T be the complementary sensitivity function that represents transfer function between the noise and the output. These two sensitivities are complementary as they add up to yield unity. Thus, the governing equations can be expressed as

$$Y(s) = TR(s) + SD(s) - TN(s) \quad (18)$$

$$E(s) = SR(s) - SD(s) + TN(s) \quad (19)$$

where T and S are given as

$$S = \frac{1}{1+PC} \quad (20)$$

$$T = \frac{PC}{1+PC} \quad (21)$$

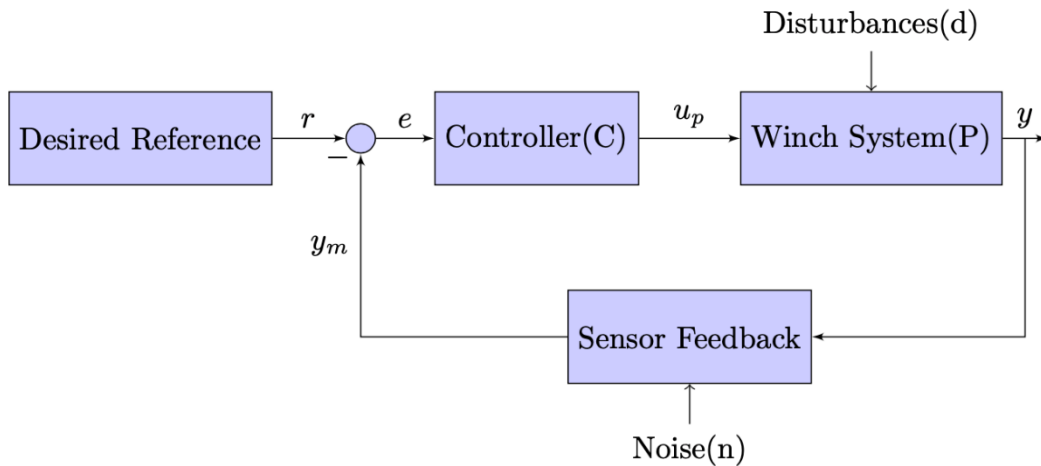


Fig. 7 Schematic diagram of closed loop winch control system

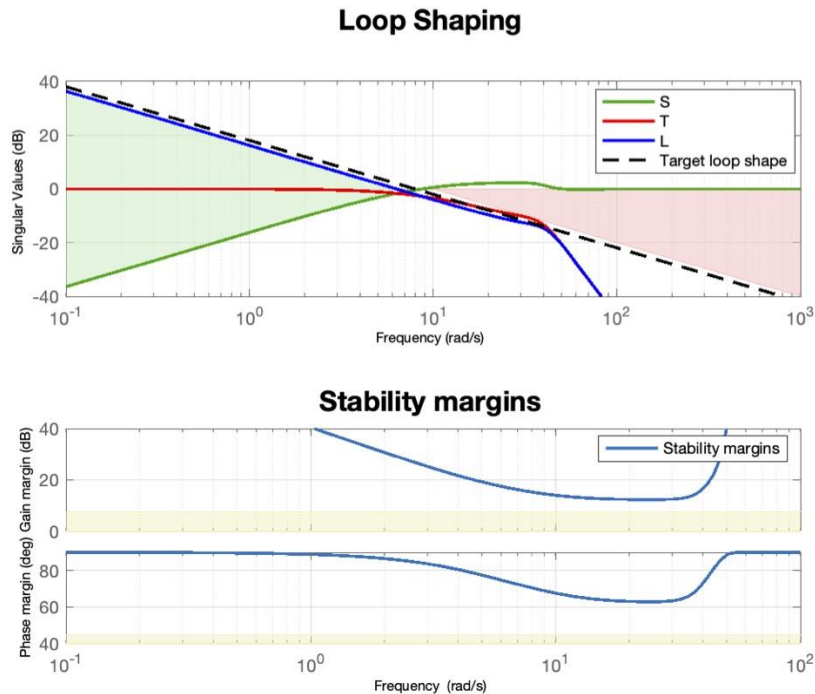


Fig. 8 Loop Shaping for tuning PD controller

The goal of this closed loop feedback system is to provide stability, disturbance rejection, and noise attenuation. At low frequencies, the sensitivity function should be small as we want a good disturbance rejection and a proper reference tracking. In the high frequency region, the complementary sensitivity function should be small as noise (predominantly composed of high frequency components) has to be attenuated. The point at which the open loop transfer function ($L=PC$) crosses the 0 dB line is the crossover frequency where we consider a trade-off between proper reference tracking, disturbance rejection, and noise attenuation.

The `looptune()` function from MATLAB was used to tune the PD controller. To design a feedback system, the open-loop transfer function (L) should be similar to an integrator with a constant slope. Its location is determined by the point at which the crossover frequency is assumed. The crossover frequency of 8 rad/s was used for the '`looptune()`' function to tune the controller gains. The value of 8 rad/s was chosen as the crossover frequency for the PD controller as it was able to provide an considerable compensation performance along with good disturbance rejection and noise attenuation. Fig. 8 shows the stability margins and the plot of S and T along with the loop transfer function L .

The dotted line in Fig. 8 represents the target loop shape whereas the blue line indicates the actual loop transfer function when the PD controller gains are tuned. Gain margin indicates how much gain it would take to make a 0 dB gain at the -180 degree phase frequency whereas phase margin indicates how much phase lag it would take to make a -180 degree phase at the 0 dB gain frequency. Thus, for the closed loop system to be stable, the system should be designed such that the crossover frequency is far away from the -180 degree phase frequency. As per Fig. 8, it can be seen that the

gain margin and the phase margin are positive and never reach the 0 dB and the 0 degree line, hence can be considered reasonably stable to process variations.

While tuning the parameters, low pass filtered derivative signal was used rather than a pure derivative as the pure derivative amplifies measurement noise. The tuned gains for the PD controller are shown below

$$K_p = 5.86, K_d = 5.46, T_f = 0.03 \quad (22)$$

where K_p , K_d are the controller gains and T_f is the time constant for noise filter. The control input for this control law in time domain is given by

$$u_p(t) = K_p e(t) + \frac{K_d}{T_f} \left(1 - \frac{e^{-t/T_f}}{T_f} \right) e(t) \quad (23)$$

4.2 LQI controller

LQI/LQR Control (Kwakernaak and Sivan 1972) is a type of optimal control problem which minimizes the cost function by providing an optimum feedback gain matrix K by penalizing the states and the control input such that there is a trade-off between set point tracking and controller effort as per our own performance requirement. LQI control has an added benefit of proper tracking for varying set point over LQR control due to integral action. It was used over pole placement control because pole placement uses pole locations to find the optimal gain matrix K , which might not be intuitive as the order of the system increase whereas LQI finds the optimal feedback matrix K based on the closed loop performance we desire. The quadratic cost function J for the optimal control problem is given by

$$J = \int_0^{\infty} (x^T Q x + u_p^T R u_p) dt \quad (24)$$

where Q and R are the tuning matrices depending on the performance requirement. The tuned values of Q and R is shown below

$$Q = \begin{bmatrix} 1 & 0 & 0 & 0 & 0 \\ 0 & 10^{-7} & 0 & 0 & 0 \\ 0 & 0 & 1 & 0 & 0 \\ 0 & 0 & 0 & 1 & 0 \\ 0 & 0 & 0 & 0 & 10^{12} \end{bmatrix} \quad R = [10] \quad (25)$$

The strict feedback control input u_p which minimizes the above cost function is given by

$$u_p = -K [x_p \quad \Delta p \quad \dot{z}_w \quad z_w \quad x_e]^T = -Kx \quad (26)$$

where K is a 1×5 matrix and x_e is the 5th state which is the integral of difference between the desired reference and state space output. A high weight of 10^{12} was provided to the 5th state as compared to the other states to emphasize low steady state error and hence result in a low net heave of the payload. The feedback matrix K is given by

$$K = R^{-1} B^T P(t) \quad (27)$$

where $P(t)$ is a positive definite solution of the Ricatti equation given by

$$A^T P(t) + P(t)A - P(t)BR^{-1}B^T P(t) + Q = -\dot{P}(t) \quad (28)$$

To tune the K matrix, the 'lqi()' function from MATLAB was used to find the optimum gain matrix K for a good tracking leading to the value

$$K = [814.2 \quad -1.02 \times 10^{-4} \quad 1.26 \times 10^3 \quad 6.124 \times 10^4 \quad -3.16 \times 10^5] \quad (29)$$

4.3 MPC

Model predictive control (Woodacre *et al.* 2018) is a discrete control algorithm that determines the optimal controller output required to reach a particular set-point by minimizing the quadratic cost function. The cost function J is given by

$$J = \sum_{i=0}^{N_p} (y + z_{\text{ship}})^T Q (y + z_{\text{ship}}) + \sum_{i=0}^{N_c} u_p^T P u_p + \sum_{i=0}^{N_c} \Delta u_p^T R \Delta u_p \quad (30)$$

$$u_{\min} \leq u_p \leq u_{\max}$$

$$N_c \leq N_p$$

where Q , P , and R are the weighting parameters (can be matrices in case of multiple inputs or outputs) for the winch output tracking error, control input, and the rate of change of control input. N_p is the prediction horizon over which the controller allows the model to evolve, N_c is the control horizon which tells how many time steps forward the control action is evaluated. In this paper, a 50 millisecond time step was used. The choice of N_c and N_p will depend on the sampling time and the time scale of the system's dynamics. For a given value of N_p , larger control horizon results in more computational complexity, whereas for a given N_c , the larger value of the prediction horizon results in less control action. Hence N_p and N_c need to be tuned depending on the requirement.

The MPC toolbox from SIMULINK was used to tune the controller which uses its internal dynamic model of the process, a cost function J over the receding (moving) horizon, and an optimization algorithm in order to minimize the cost function J by altering the control input. The main difference between model predictive control (MPC) and LQI is that MPC performs cost optimization in a receding time window, whereas LQI optimizes the cost in a fixed time window. Thus, MPC may obtain a sub optimal solution as it solves the optimization in a smaller time window as compared to LQI. However, MPC has a benefit that it can handle hard constraints, which is the main demerit of LQI. The tuned parameters for MPC are shown in Table 3. A higher weight of 7 was provided to the compensated heave at the winch in order to make the controller more aggressive towards the closed loop performance.

Table 3 Tuned Values for MPC

Parameter	N_p	N_c	Q	P	R
Value	20	4	7	0.1	0.01

4.4 Sliding mode controller

Sliding mode control (Khalil and Grizzle 2002) is a nonlinear control strategy that changes the dynamics of a nonlinear system with the help of a discontinuous control signal that forces the system to slide along a cross-section of the system's normal behaviour. The most prominent feature of sliding mode control (SMC) is that it is insensitive to parametric uncertainty and external disturbances during the sliding mode. A sliding mode controller can stabilize the trajectory of a system. There are two steps in the SMC design. The first step is designing a sliding surface so that the plant restricted to the sliding surface has a desired system response. This means the state variables of the plant dynamics are constrained to satisfy another set of equations that define the so called sliding surface. The second step is constructing a switching feedback gains necessary to drive the plant's state trajectory to the sliding surface. These constructions are built on the generalized Lyapunov stability theory (Khalil and Grizzle 2002). The sliding mode surface S is expressed as

$$S = \sigma = \left(\frac{d}{dt} + k\right)^{n-1} e \quad (31)$$

where n is the number of states of the system, $e = z_w - r$ is the error between the output of the winch and the desired reference, and k is a positive parameter which is chosen based on the performance we desire. The equivalent control input u_{eq} is obtained by making the derivative of S to be zero.

$$\dot{S} = 0 \quad (32)$$

The switching control is given by

$$u_s = k_p \text{sgn}(S) + \alpha S \quad (33)$$

where k_p is the controlled gain, α is a constant positive gain for exponential reaching law, and $\text{sgn}(\cdot)$ is the signum function. An exponential reaching law was used in order for the system to reach the sliding surface faster. Therefore, the overall control law $u_p = u_{eq} + u_s$ is then obtained by setting

$$\frac{d}{dt} \left(\left(\frac{d}{dt} + k\right)^{n-1} e \right) = -k_p \text{sgn}(S) - \alpha S \quad (34)$$

to solve for the control input u_p . In our model $n = 4$, which yields S to be

$$S = \ddot{e} + 3k\ddot{e} + 3k^2\dot{e} + k^3e \quad (35)$$

Now equating

$$\dot{S} = -k_p \text{sgn}(S) - \alpha S \quad (36)$$

we have

$$u_p = k_p \text{sgn}(S) + \alpha S + \ddot{r} + k_3(\dot{r} - \dot{z}_w) + k_2 \left(\ddot{r} + \frac{\dot{z}_w b}{mr^2 + J_w} + \frac{D_m \eta_m k r \Delta p}{(mr^2 + J_w)} \right) \quad (37)$$

$$+ \left(\frac{D_m b \eta_m k r}{(mr^2 + J_w)^2} \right) \left(\frac{2D_p k_{oil} \omega_p x_p}{V_c} - \frac{2D_m k k_{oil} \dot{z}_w}{V_c r} \right) + \frac{2D_m D_p \eta_m k k_{oil} r \omega_p x_p}{T_p V_c (mr^2 + J_w)}$$

$$\begin{aligned}
 & + \left(\frac{b^2}{(mr^2 + J_w)^2} - \frac{2D_m^2 \eta_m k^2 k_{oil}}{V_c (mr^2 + J_w)} \right) \left(\frac{\dot{z}_w b}{mr^2 + J_w} + \frac{D_m \eta_m k r \Delta p}{mr^2 + J_w} \right) \\
 & - k_1 \left(\frac{b(\dot{z}_w b + D_m \eta_m k r \Delta p)}{(mr^2 + J_w)^2} - \ddot{r} + \frac{D_m \eta_m k r (2r D_p k_{oil} \omega_p x_p - 2D_m k k_{oil} \dot{z}_w)}{V_c r (mr^2 + J_w)} \right)
 \end{aligned}$$

where $k_1 = 3k$, $k_2 = 3k^2$ and $k_3 = k^3$ respectively. The parameters of the sliding mode control law should be chosen in order to enhance the performance of the controlled system. Here k , k_p and α were tuned and $k = 27$, $k_p = 70$, and $\alpha = 1$ were found to yield to good control. The SMC however has a drawback that not all derivatives or r can be practically measured. Also, numerical calculation of these derivatives will cause numerical errors to be introduced and can have a detrimental effect on the control performance. Therefore, even though SMC is mathematically elegant, it can be hard to implement practically.

5. Simulation results

In this paper four control strategies i.e. PD, MPC, LQI, and SMC are compared to understand the advantages and limitations of the control algorithms. The following three cases were examined:

1. Heave compensation with no disturbance and no measurement noise
2. Heave compensation with disturbance but no noise
3. Heave compensation with noise but no disturbance

Fig. 9 shows the plot of uncompensated motion time history for these three sea states. The RMS value of uncompensated net heave at the winch for slight, moderate and rough sea states evaluated from a 1000 seconds time history were found to be 0.0262 m, 0.2913 m, and 0.9712 m respectively.

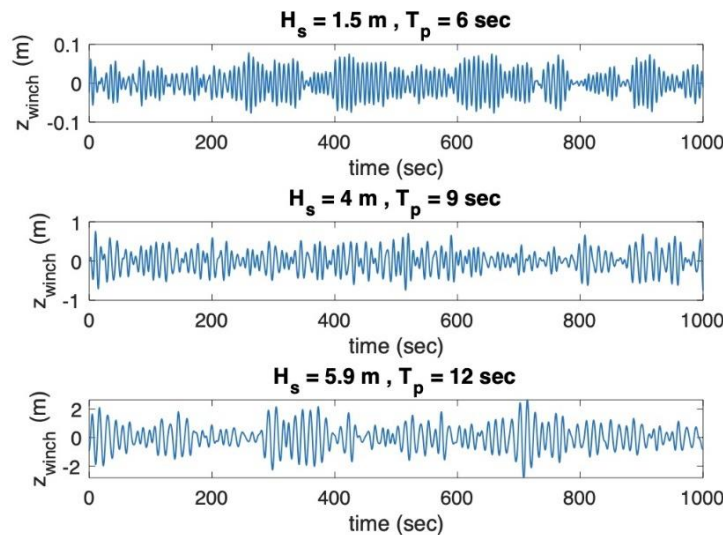


Fig. 9 Uncompensated motion time history at the winch for three sea states

Table 4 Slight Sea State

Controller	rms(Compensated Motion)	Heave Compensation
PD	0.0035 m	86.64 %
MPC	0.0026 m	90.07 %
LQI	0.0045 m	82.82 %
SMC	0.0009 m	96.56 %

Table 5 Moderate Sea State

Controller	rms(Compensated Motion)	Heave Compensation
PD	0.0298 m	89.77 %
MPC	0.0222 m	92.38 %
LQI	0.0376 m	87.09 %
SMC	0.0273 m	90.63 %

Table 6 Rough Sea State

Controller	rms(Compensated Motion)	Heave Compensation
PD	0.0767 m	92.1 %
MPC	0.0574 m	94.09 %
LQI	0.0973 m	89.98 %
SMC	0.0725 m	92.53 %

5.1 Heave compensation with no disturbance and no measurement noise

Table 4-6 show the analysis of the compensated performance for all the controllers. In this study, heave compensation was defined as the ratio of the difference between the RMS value of uncompensated and compensated net heave at the winch to the RMS value of uncompensated net heave at the winch.

As shown in Fig. 10(a), SMC was able to provide the best compensation for slight sea state. However, in practical applications, SMC can cause a lot of wear and tear to actuators' mechanical equipment due to its discontinuous control signal.

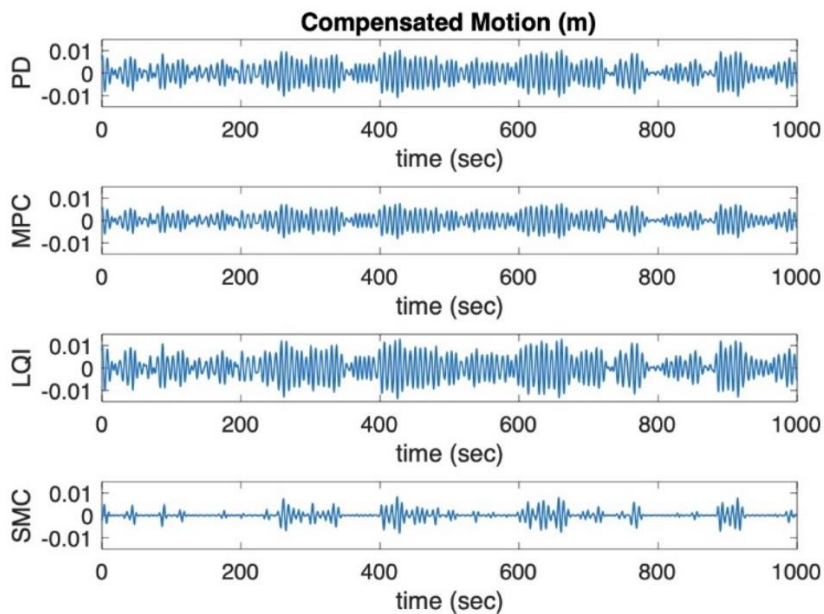
LQI control demonstrated the least compensation for all the three sea states. Since LQI is based on a linear model of the plant, it could not compensate heave motion when the normalized swash angle attained saturation. This scenario occurred in the rough sea state at about $t = 250$ seconds when the uncompensated net heave motion at the winch experienced a relatively sharp increase in amplitude (Fig. 9) resulting in normalized swash angle saturation as seen in Fig. 11. The poor compensation of heave motion during this period is evident from the compensated motion plot shown in Fig. 10(c). The controller could not recover until $t = 450$ seconds when the uncompensated heave motion magnitude reduced.

A similar larger uncompensated heave motion was also experienced at about $t = 700$ seconds. However, in this case LQI did not reach saturation and was able to compensate the heave motion better (Fig. 10(c)). This can be attributed to the rate of increase in uncompensated heave motion. It can be seen that at $t = 250$ seconds, the uncompensated heave motion envelope experiences a sharp jump whereas the rise at $t = 700$ seconds is gradual. In a sharp jump case, the controller attempts to compensate by increasing the control input sharply and hence resulting in a saturation. However, when the increase is gradual, the control input also increases gradually and hence avoids saturation.

MPC was found to outperform other strategies in terms of compensation for moderate and rough sea states. It was also found that MPC required the minimal control input to achieve such compensation as compared to other strategies. However, MPC does have a disadvantage that, it performs an online optimization and hence requires considerable online computation power for real time applications.

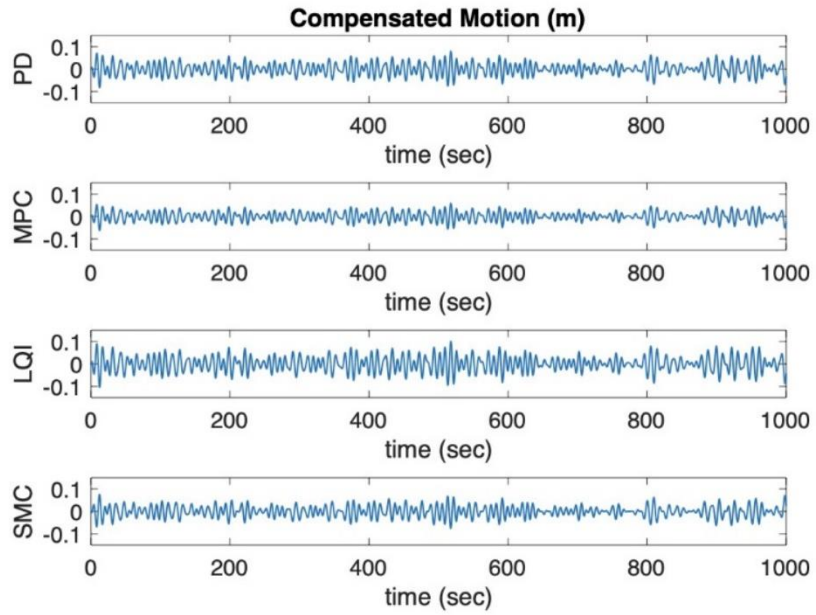
PD control showed intermediate compensation for all the three sea states in comparison to all other controllers.

Fig. 12 shows the power spectral density of the compensated motions for various strategies in moderate sea state. It can be seen that in terms of compensation, MPC has the best performance followed by SMC, PD and LQI. Fig. 13 shows the ability of each strategy in tracking an offset for moderate sea state for wave incident angles of 90, 135 and 180 degrees. It was found that all the controllers were good at tracking the offset except LQI. LQI demonstrated long overshoots when the offset was introduced and removed. This can again be explained due to the saturation of swash angle when a sudden offset of 1 m is applied or removed.

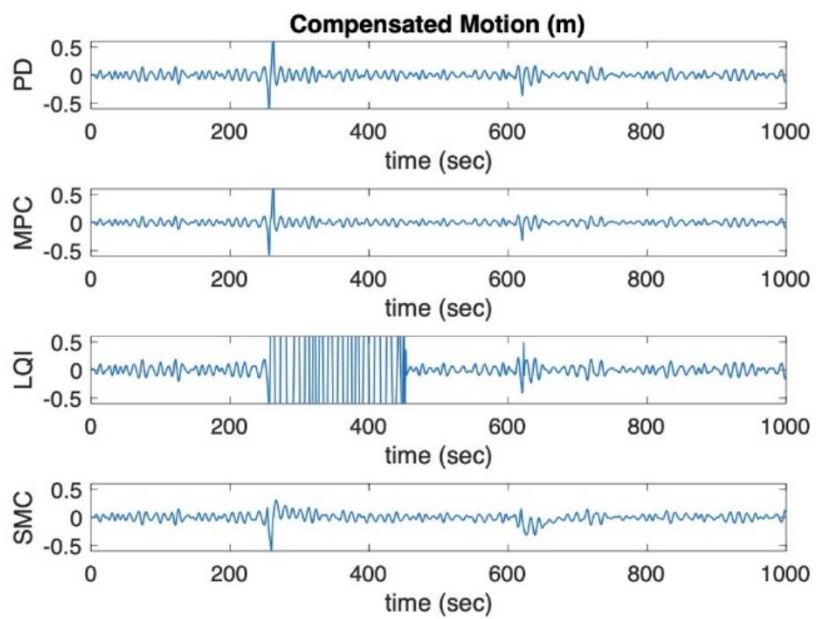


(a)

Continued-



(b)



(c)

Fig. 10 (a) $H_s = 1.5$ m, $T_p = 6$ sec (b) $H_s = 4$ m, $T_p = 9$ sec (c) $H_s = 5.9$ m, $T_p = 12$ sec

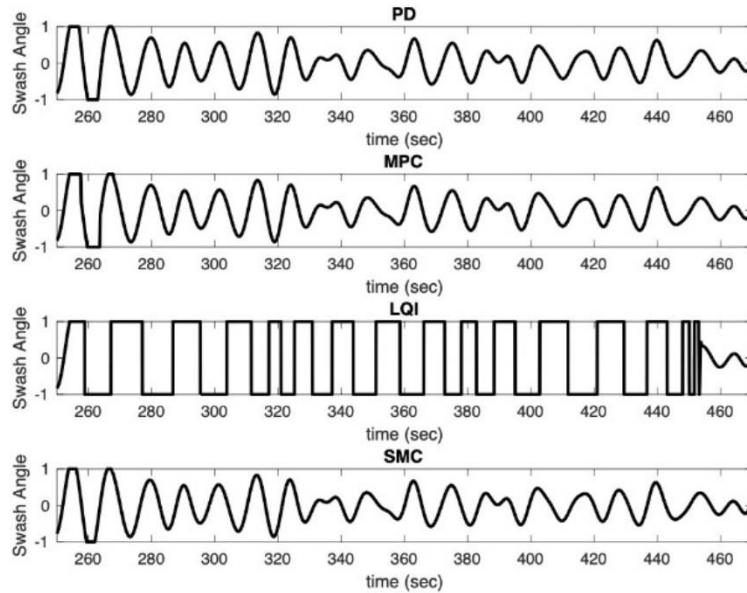


Fig. 11 Normalized Swash Angle from 250 sec to 470 sec for $H_s = 5.9 \text{ m}, T_p = 12 \text{ sec}$

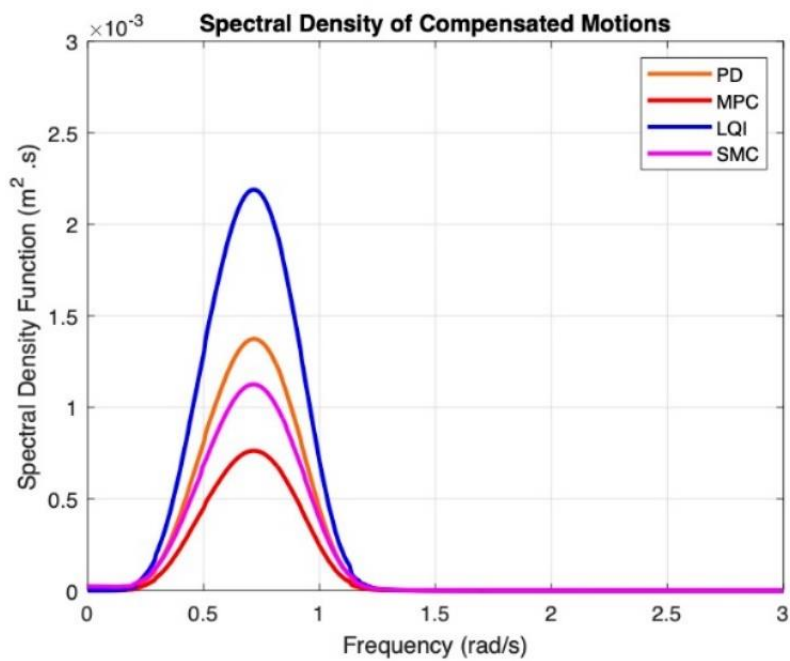
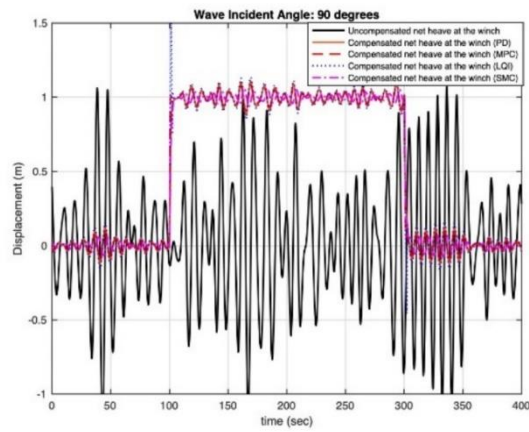
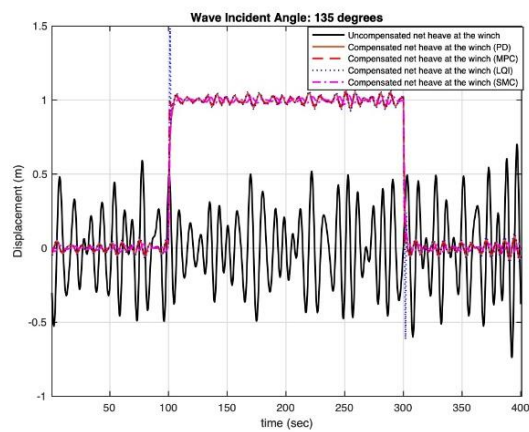


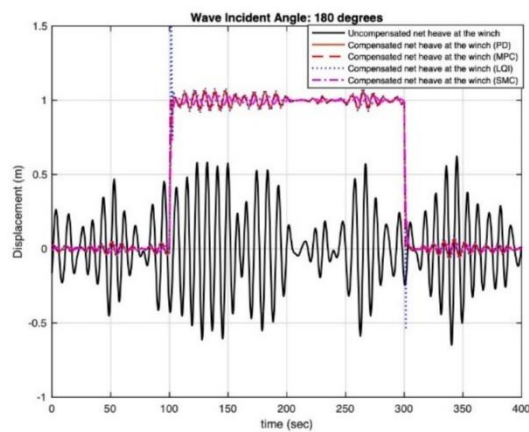
Fig. 12 Spectrum of compensated motions for various controllers with no disturbance and no noise for $H_s = 4 \text{ m}, T_p = 9 \text{ sec}$



(a)



(b)



(c)

Fig.13 Ability of the controller to track offset for $H_s = 4$ m, $T_p = 9$ sec

5.2 Heave compensation with disturbance and no noise

In order to analyze the ability of the controllers to reject disturbance, the disturbance time history was generated with a constant spectrum of spectral density value 10^{-3} between a cut in and cut off frequencies of 0 rad/s and 0.5 rad/s respectively to perform the simulations. In this study we assume that the disturbance enters the system only through the third state (heave velocity \dot{z}_w). Since the ability of controllers to reject disturbances is independent of sea state, the simulation results were analyzed only for the moderate sea state.

Fig. 14 shows the power spectral density of the disturbance and compensated motion time history for each of the strategies when the disturbance was included. It can be seen from Fig. 14 that SMC was found to be most sensitive to disturbance. Other than SMC, all the controllers were reasonably good at rejecting disturbances.

5.3 Heave compensation with noise and no disturbance

In order to analyze the ability of the controllers to attenuate measurement noise, two cases were conducted: one with a low measurement noise having spectral density value of 10^{-6} with a cut in and cut off frequency of 3.14 rad/s and 50 rad/s respectively and other with a high measurement noise having spectral density value of 10^{-3} with the same cut in and cut off frequencies. In this study, the noise was added only to the reeled length of the rope (i.e. z_w) of the winch model and given as a feedback to the controller. The signal to noise ratio (SNR) is usually defined in decibels as

$$SNR = 10\log_{10}\left(\frac{\sigma_{signal}^2}{\sigma_{noise}^2}\right) = 20\log_{10}\left(\frac{\sigma_{signal}}{\sigma_{noise}}\right) \quad (38)$$

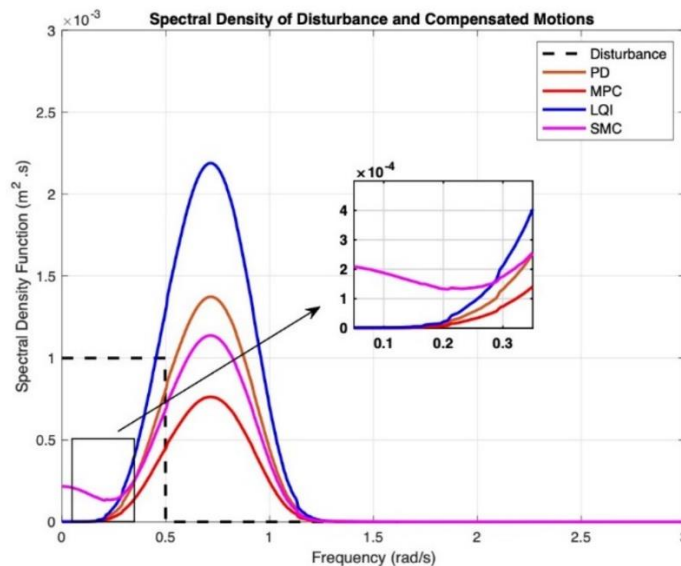


Fig.14 Ability of the controller to reject disturbance for $H_s = 4 \text{ m}, T_p = 9 \text{ sec}$

In this study σ_{signal} is taken as the RMS value of the uncompensated net heave motion at the winch and σ_{noise} is taken as the RMS value of the noise. A constant noise spectral density of 10^{-6} between 3.14 rad/s and 50 rad/s corresponds to a SNR value of 1810 dB for the moderate sea state and in this case, the system does not observe saturation due to noise. A constant noise spectral density of 10^{-3} between 3.14 rad/s and 50 rad/s corresponds to a SNR value of 1.81 dB for the moderate sea state and in this case, the normalized swash angle experiences saturation due to noise. Fig. 15 shows the plot of the output $y(t) \equiv z_w(t)$ and the measured output $y_m(t) \equiv z_w(t) + n(t)$ for these two cases for a duration of 200 seconds.

Since measurement noise typically does not vary significantly with a change in sea state, the ability of the controllers to attenuate noise was only analysed for the moderate sea state.

5.3.1 With low measurement noise

Fig. 16 shows the power spectral density of the noise and compensated motion time history for each of the strategy when a low measurement noise was included. As per Fig. 16, SMC was totally insensitive to measurement noise. PD controller was found to be good at attenuating noise as compared to LQI before 8 rad/s. However, LQI controller was found to outperform PD controller in attenuating noise after 8 rad/s. It can be seen from Fig. 16 that at higher frequencies optimal control had an edge over classical control in terms of noise attenuation. MPC showed an odd behaviour in which the measurement noise amplified and started to attenuate noise only after 20 rad/s. However, the peak of the MPC at 20 rad/s can be decreased and shifted to the left by decreasing the weights to $Q = 1$ for the compensated motion at the winch but this results in a significant decrease in heave compensation performance of about 60%.

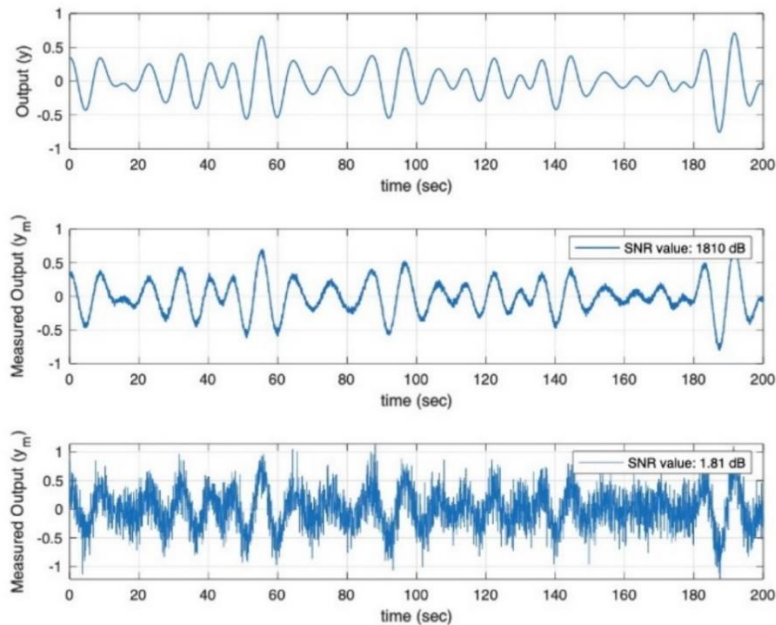


Fig. 15 Output and Measured Outputs for two noise cases

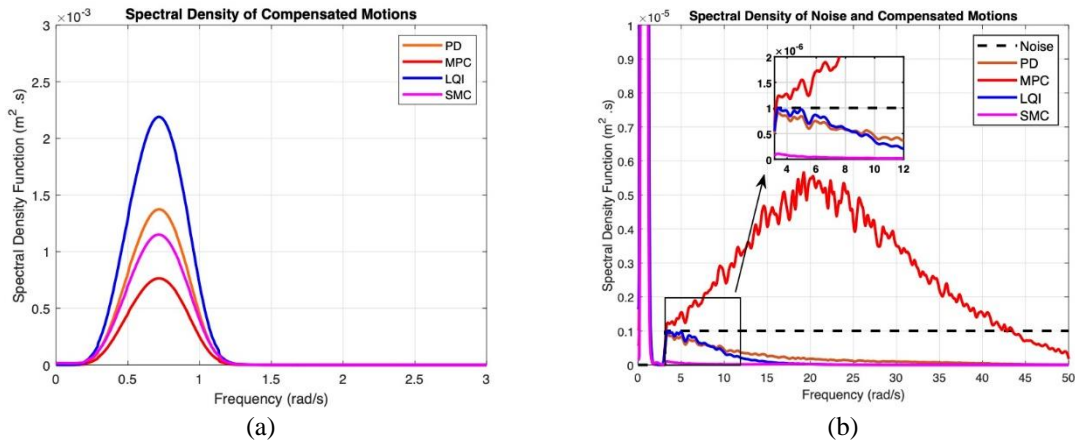


Fig. 16 Spectrum of compensated motions for low noise (SNR = 1810 dB) plotted between (a) 0 and 3 rad/s (b) 0 and 50 rad/s

5.3.2 With high measurement noise

Fig. 17 shows the power spectral density of the noise and compensated motion time history for each of the strategy when a high measurement noise was included. Saturation in the normalized swash angle was observed for MPC and PD controller when a high measurement noise was added.

As per Fig. 17(b), all the controllers were reasonably good at attenuating measurement noise. However due to saturation in the normalized swash angle, MPC and PD controller showed an high peak in spectrum between 0 and 1.5 rad/s. This means that the compensation is significantly affected for PD and MPC when a large noise is present in the system. However, for LQI and SMC a strong noise has very minimal effect on performance and their ability to attenuate noise even when high measurement noise is present in the feedback signal.

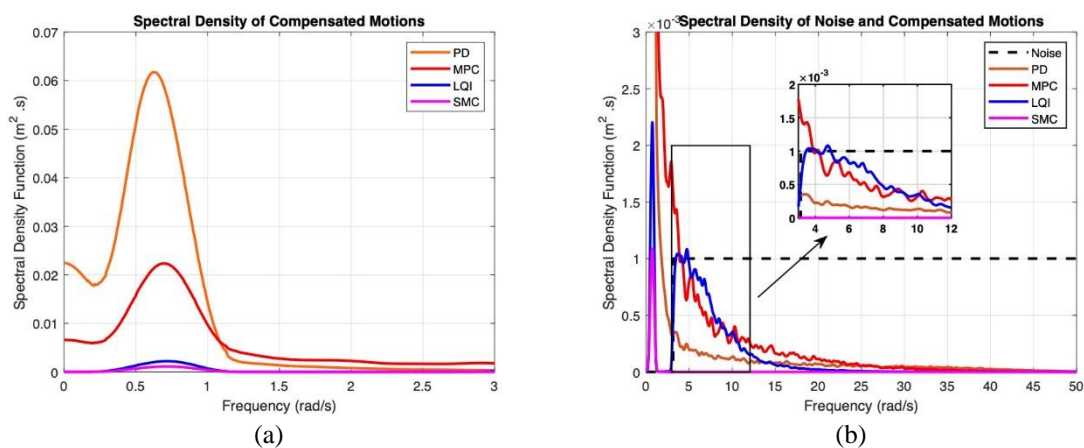


Fig. 17 Spectrum of compensated motions for high noise (SNR = 1.81 dB) plotted between (a) 0 and 3 rad/s (b) 0 and 50 rad/s

6. Conclusions

In this paper, four control strategies - PD (Proportional Derivative Control), LQI (Linear Quadratic Integral Control), MPC (Model Predictive Control) and SMC (Sliding Mode Control) - are implemented for achieving active heave compensation. The four control strategies are described in detail and their performances are compared and analyzed in keeping a payload at a regulated height while rejecting the net heave at the winch arising from ship motions at sea. When no noise or disturbance is present, SMC showed the best heave compensation while in moderate and rough sea states MPC performed better. Although SMC could attenuate noise very well owing to the chosen dynamics on the sliding surface, it could not effectively reject disturbances in the plant. MPC on the other hand could reject disturbances well, but could not attenuate low noise added to the feedback signal. LQI controller was found to have the least compensation performance among all the controllers for all the three sea states. It also failed to compensate motion in severe sea state and was affected considerably by saturation dynamics. However, it was able to perform decent disturbance rejection and noise attenuation. Since measurement noise is low in practical applications, PD control tuned with loop tuning exhibited a good compromise between all the control strategies with a decent performance across disturbance rejection, noise attenuation and reference tracking.

References

- Atmanand, M. and Ramadass, G. (2017), "Concepts of Deep-Sea Mining Technologies", in "Deep-Sea Mining", pages 305–343, Springer, Berlin, Germany.
- Falzarano, J., Somayajula, A. and Seah, R. (2015), "An overview of the prediction methods for roll damping of ships", *Ocean Syst. Eng.*, **5**(2), 55-76.
- Fang, M.C., Lin, Y.H. and Wang, B.J. (2012), "Applying the PD controller on the roll reduction and track keeping for the ship advancing in waves", *Ocean Eng.*, **54**, 13–25.
- Fossen, T.I. (2011), *Handbook of Marine Craft Hydrodynamics and Motion Control*, John Wiley & Sons, NJ, USA.
- Fossen, T.I. and Strand, J.P. (2001), "Nonlinear passive weather optimal positioning control (WOPC) system for ships and rigs: experimental results", *Automatica*, **37**(5), 701-715.
- Galuppini, G., Magni, L. and Raimondo, D.M. (2018), "Model predictive control of systems with deadzone and saturation", *Control Eng. Practice*, **78**, 56-64.
- Grimble, M., Patton, R. and Wise, D. (1980), "The design of dynamic ship positioning control systems using stochastic optimal control theory", *Optimal Control Appl. Methods*, **1**(2), 167-202.
- Guha, A. (2016), "Development and application of a potential flow computer program: determining first and second order wave forces at zero and forward speed in deep and intermediate water depth", Ph.D. Dissertation, Texas A&M University, College Station, TX.
- Guha, A., Somayajula, A. and Falzarano, J. (2016), "Time domain simulation of large amplitude motions in shallow water", in "21st SNAME Offshore Symposium", Society of Naval Architects and Marine Engineers, Houston, TX.
- Hatleskog, J.T. and Dunnigan, M.W. (2007), "Passive compensator load variation for deep-water drilling", *IEEE J. Oceanic Eng.*, **32**(3), 593-602.
- Jakubowski, A. and Milecki, A. (2018), "The investigations of hydraulic heave compensation system", in "Conference on Automation", Springer, Berlin, Germany.
- Khalil, H.K. and Grizzle, J.W. (2002), *Nonlinear Systems*, volume 3, Prentice Hall, Upper Saddle River, NJ, USA.
- Korde, U.A. (1998), "Active heave compensation on drill-ships in irregular waves", *Ocean Eng.*, **25**(7), 541-561

- Kwakernaak, H. and Sivan, R. (1972), *Linear Optimal Control Systems*, volume 1, Wiley-InterScience, New York, USA.
- Li, J.W., Ge, T. and Wang, X.Y. (2012), "Output Feedback Control for an Active Heave Compensation System", in "Computer, Informatics, Cybernetics and Applications", Springer, Berlin, Germany.
- Li, M., Gao, P., Zhang, J., Gu, J. and Zhang, Y. (2018), "Study on the system design and control method of a semi-active heave compensation system", *Ships Offshore Struct.*, **13**(1), 43-55.
- Li, Z., Ma, X., Li, Y., Meng, Q. and Li, J. (2019), "ADRC-ESMPC active heave compensation control strategy for offshore cranes", *Ships Offshore Struct.*, 1-9.
- Ni, J., Liu, S., Wang, M., Hu, X. and Dai, Y. (2009), "The simulation research on passive heave compensation system for deep sea mining", *Proceedings of the 2009 International Conference on Mechatronics and Automation*, 5111-5116, IEEE.
- Richter, M., Schaut, S., Walser, D., Schneider, K. and Sawodny, O. (2017), "Experimental validation of an active heave compensation system: estimation, prediction and control", *Control Eng. Practice*, **66**, 1-12.
- Somayajula, A. and Falzarano, J. (2016), "Estimation of roll motion parameters using R-MISO system identification technique", *Proceedings of the 26th International Offshore and Polar Engineering (ISOPE 2016), Conference*, International Society of Offshore and Polar Engineers (ISOPE), Rhodes, Greece.
- Somayajula, A. and Falzarano, J. (2017a), "Application of advanced system identification technique to extract roll damping from model tests in order to accurately predict roll motions", *Appl. Ocean Res.*, **67**, 125-135.
- Somayajula, A. and Falzarano, J. (2017b), "Critical assessment of reverse-MISO techniques for system identification of coupled roll motion of ships", *J. Marine Sci. Technol.*, **22**(2), 231-244.
- Somayajula, A., Guha, A., Falzarano, J., Chun, H.H. and Jung, K.H. (2014), "Added resistance and parametric roll prediction as a design criteria for energy efficient ships", *Ocean Syst. Eng.* **4**(2), 117-136.
- Somayajula, A.S. (2017), "Reliability Assessment of Hull Forms Susceptible to Parametric Roll in Irregular Seas", Ph.D. Dissertation, Texas A&M University, College Station, TX.
- Sonnenburg, C.R. and Woolsey, C.A. (2013), "Modeling, identification, and control of an unmanned surface vehicle", *J. Field Robot.*, **30**(3), 371-398.
- Sørensen, A.J. (2005), "Structural issues in the design and operation of marine control systems", *Annu. Review. Control*, **29**(1), 125-149.
- Woodacre, J. (2015), "Model-predictive control of a hydraulic active heave compensation system with heave prediction", Ph.D. Dissertation, Dalhousie University, Nova Scotia, Canada.
- Woodacre, J., Bauer, R. and Irani, R. (2015), "A review of vertical motion heave compensation systems", *Ocean Eng.*, **104**, 140-154.
- Woodacre, J., Bauer, R. and Irani, R. (2018), "Hydraulic valve-based active-heave compensation using a model predictive controller with non-linear valve compensations", *Ocean Eng.*, **152**, 47-56.
- Zhao, L., Roh, M.I. and Ham, S.H. (2018), "Performance analysis of an active heave compensation system on an offshore supply vessel using the hardware-in-the-loop simulation", *J. Marine Sci. Technol.*, **26**(5), 678-691.